2. Study on Cavitation Erosion

Ryuichi SATO*, *Member*, Shin TAMIYA*, *Member*, Hiroharu KATO*, *Member*

(*From J.S.N.A. Japan Vol. 134, Dec. 1973*)

Summary

In this paper, authors conducted experimental investigations on cavitation damage to specimens of pure aluminum placed in a venturi type cavitation tunnel.

The main object of experiments is to confirm the relation between damage intensity and flow velocity.

Conclusions obtained are as follows;

(1) Cavitation damage intensity is largely affected by flow velocity, for instance, the number of erosion pits varies with the 5th to 6th power of flow velocity.

(2) Erosion pits are generated near the end of fixed-cavity.

(3) Distribution of erosion pits are supposed to be caused by difference of initial radius of a collapsing bubble and oscillatory variation of length of fixed-cavity.

Simplified equation of bubble radius is solved numerically. From the calculation of pressure field around a collapsing bubble, following results are obtained;

(4) Maximum pressure on bubble wall varies with the 11th power of flow velocity.

(5) Maximum velocity of bubble wall varies with the 5th power of flow velocity.

(6) On the assumption that damage intensity increases in proportion to impulse provided to the surface of specimens, these calculations show good agreement with experimental results.

Preface

Erosion is one of the most serious problem concerning cavitation generated on marine propellers. Though many experiments have been conducted since many years, we are not yet given systematized theory to explain the phenomenon. Cavitation erosion is connected not only with hydrodynamics but also with metal science, and approaches from these two fields are considered inevitable to reveal its property.

In this paper we attempt to develop hydrodynamic approach and investigate flow velocity effect on damage intensity.

1. Cavitation Erosion Test

1.1. *Test Equipment and Specimens*

There are two methods to produce cavitation erosion on surfaces of materials. One is to hit materials with high speed water flow or to vibrate specimens in test liquid at high frequency. By these methods we can produce cavitation erosion rapidly, and these are useful to compare or determine erosion resistance of materials. But with these methods we are confronted with a difficulty that the relation is not clear between actual cavitation erosion and that produced in these experiments.

The other is flow-produced method, in which we set specimens in a venturi type cavitation tunnel and expose them to high speed flow. This method makes it possible to investigate relations between damage intensity and some flow parameters. On the other hand it must take long experimental time to produce cavitation erosion in usual cavitation tunnels.

In this paper we adopt flow-produced

* University of Tokyo

method to get informations on cavitation erosion relating to hydrodynamic properties of the flow, that is, relation between damage intensity and flow velocity and distribution of erosion pits along the main flow.

Experiments were conducted in the high speed cavitation tunnel of University of Tokyo. This is a venturi type cavitation tunnel with circular test section of 30 mm diameter. This diameter enables us to get maximum flow velocity up to 80 m/s which was very useful to observe cavitation erosion in a short time.[1),2)]

Cavitation erosion is largely affected by gas contents of test water. In this series of experiments we used water with low gas contents to produce cavitation erosion speedily. Tap water was degassed in the depressurizing tank in 2 hours up to the under-saturate condition ($\alpha/\alpha_s \doteqdot 0.6$).

Fig. 1 shows the dimensions of typical specimens. For the rapid generation of cavitation erosion test specimens are made of pure aluminum whose composition is listed in Table 1. Other soft material, lead for example, was considered too soft to be tooled.

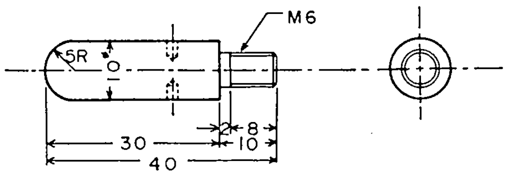

Fig. 1 Dimensions of typical specimens

Table 1 Composition of pure aluminum

Al	>	99.8%
Cu	<	0.02%
Si+Fe	<	0.20%

In order to remove the effects of work hardening from the surface of the test pieces, they were annealed in Argon gas at 400°C in an electric furnace in one hour. After annealing, Brinell hardness of the surface was measured as about 23 which was suitable for the experiments. The specimens were polished with a buffer for easy observation of erosion pits.

1.2. *Experimental Conditions*

For the investigation of the flow velocity effect, seven conditions listed in Table 2 were selected. From preliminary experiments the exposure time of each condition was determined to generate approximately the same amount of cavitation erosion. The length of the fixed-cavity was 10 mm throughout the entire range of experiments. It was maintained by controlling the tunnel static pressure and checked afterwards with photographs.

Table 2 Experimental conditions

No. of specimen	V(m/s)	l(mm)	P (kg/cm²)	exposure time
7	30	9.6	1.04	5.0 hrs
8	40	9.6	2.26	1.0 hrs
12	50	10	4.55	15 min
5	50	10	4.78	30 min
10	50	10	4.60	60 min
9	60	10.6	6.93	10 min
6	70	10	10.15	5 min

In these experiments variation of flow velocity has so large effects on the appearance of the fixed-cavity, even if the cavitation number is kept constant, that the condition of constant fixed-cavity length was prefered to that of constant cavitation number.

Three test specimens numbered 12, 5 and 10 were prepared for the observation of the effect of exposure time on damage intensity.

1.3. *Microscopic Observation of Cavitation Erosion*

Along the straight mother line through the punch mark on the specimen surface, as shown in Fig. 2, micrographics were taken before and after each test with the metallurgical microscope shown in Fig. 3. After making prints of 100 magnifications, then

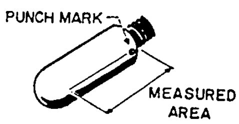

Fig. 2 Microscope field

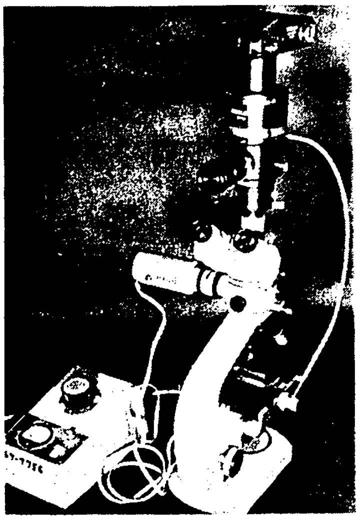

Fig. 3 Metallurgical microscope

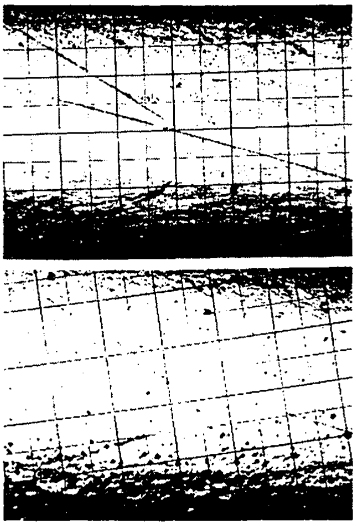

Fig. 4 Erosion pits (V=30 m/s)

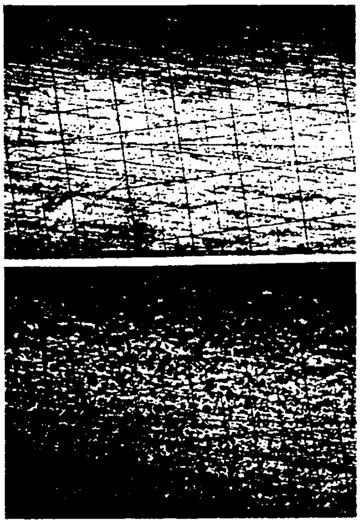

Fig. 5 Erosion pits (V=40 m/s)

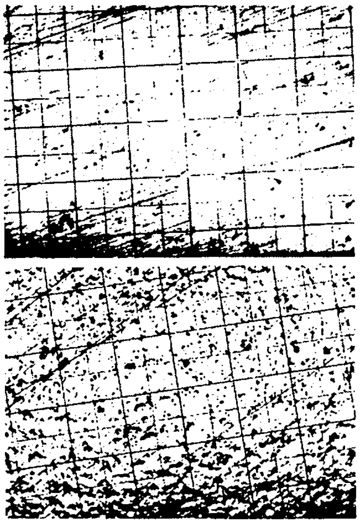

Fig. 6 Erosion pits (V=50 m/s, 30 min)

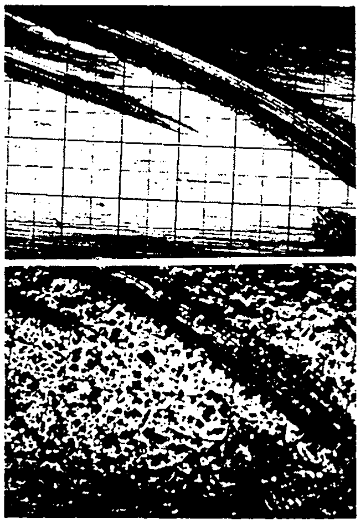

Fig. 7 Erosion pits (V=60 m/s)

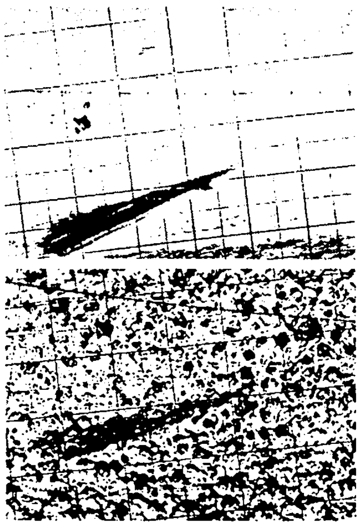

Fig. 8 Erosion pits (V=70 m/s)

connecting them, it is possible to obtain a continuous micrographics of the specimen surface, from which the number of erosion pits can be counted. In Fig. 4 through 8, typical micrographics are shown. The upper shows the specimen surface before experiment and the lower shows after the exposure. Each pair shows almost the same position on the specimen surface.

1.4 *Surface Roughness Measurements*

The surface roughness of the test specimens was measured to obtain the depth of erosion pits after each test. Fig. 9 shows an outline of the measurement. The measured

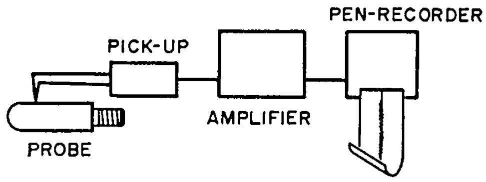

Fig. 9 Outline of surface roughness measurement

Table 3 Average depth of erosion pits

No. of specimen	V(m/s)	exposure time	average depth (μ)
7	30	5 hrs	0.189
8	40	1 hrs	0.176
12	50	15 min	0.214
5	50	30 min	0.147
10	50	60 min	0.287
9	60	10 min	0.260
6	70	5 min	0.401

Table 4 Classification of pits

d (mm)	$d<3\times10^{-2}$	$3\times10^{-2}\leq d<5\times10^{-2}$	$5\times10^{-2}\leq d$
d_{mi} (mm)	1×10^{-2}	4×10^{-2}	5×10^{-2}
number of pit ($1/10^{-2}\,mm^2$)	N_1	N_2	N_3

area is the same as the microscope field in Fig. 2. Magnification range was 2,000 X and 5,000 X. With these high magnifications the waviness of specimen surface must be removed carefully. The average depth of the erosion pits are indicated in Table 3 ranging from 0.15 to 0.40 μ with a tendency to increase with flow velocity.

1.5 *Damage Intensity Parameters*

Following three parameters are adopted in this paper indicate damage intensity quantitatively.

(1) The number of erosion pits per unit area
(2) Area erosion rate
(3) Volume loss rate

Though the weight loss of each specimens is another effective parameter, lack of a micro balance capable of measuring so long lost weight as experienced in our experiments made it impossible to adopt this parameter.

1.5.1 *Number of Erosion Pits*

Total number of erosion pits were counted irrespective of their size to obtain the number

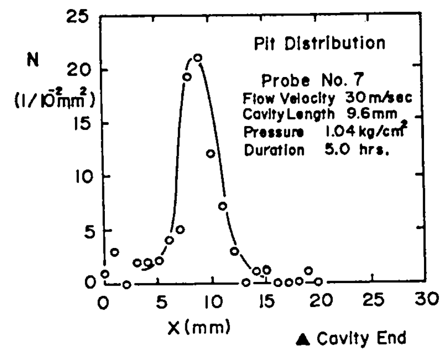

Fig. 10 Pit distribution

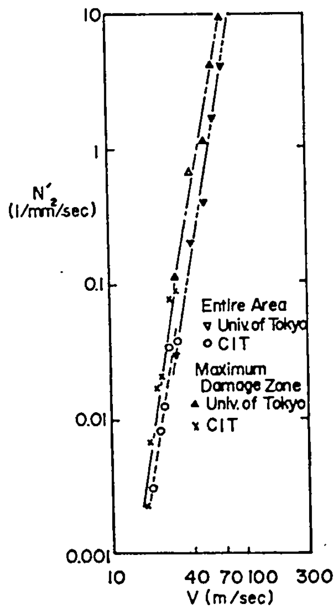

Fig. 11 Damage intensity N'

of pits per 10^{-2} mm^2, N [1/10^{-2} mm^2]. On the assumption that the time rate of generation of erosion pits is constant, the erosion rate N' [1/mm^2/sec] is calculated from N. Fig. 10 shows the distribution of erosion pits in the direction of the main flow at $V=30$ m/s. The mark ▲ in Fig. 10 indicates the mean position of the fixed-cavity end determined by photographs. The horizontal axis shows the distance from the start point of the parallel part of the test specimen.

Fig. 11 shows the flow velocity effect on damage intensity indicated by N'. N' was also adopted in erosion test at CIT, their result being shown also in Fig. 11[3].

1.5.2. *Area Erosion Rate*

Erosion pits are divided into three classes according to their diameter as shown in Table 3. Denoting the sum of the area of erosion pits in each class $S_{\mathrm{ero}\,i}$ $(i=1,2,3)$, total eroded area S_{ero} is calculated as follows.

$$S_{\mathrm{ero}} \cong \sum_{i=1}^{3} S_{\mathrm{ero}\,i}$$
$$= \frac{\pi}{4} \sum_{i=1}^{3} (d_{m}{}^2{}_i \cdot N_i \cdot 10^2)$$
$$= \frac{\pi}{4} 10^{-2} (N_1 + 16\,N_2 + 25\,N_3) \quad [\mathrm{mm}^2]$$

where $d_{m\,i}$: mean diameter of erosion pit in class i

Introducing the eroded area ratio k defined as

$$k = \frac{\text{(eroded area)}}{\text{(total area)}} \times 100 \qquad [\%]$$

then we obtain the following expression.

$$k = S_{\mathrm{ero}} / \mathrm{mm}^2 \times 100 \qquad [\%]$$

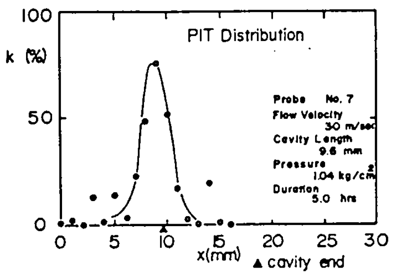

Fig. 12 Pit distribution

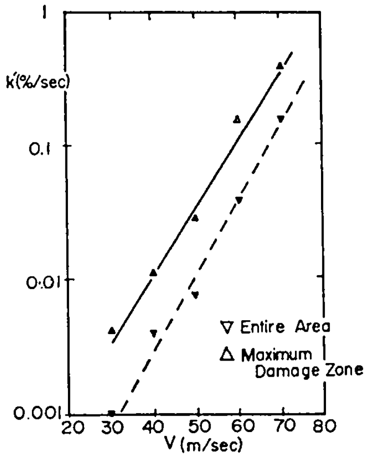

Fig. 13 Damage intensity k'

k indicates the eroded area ratio in %.

Dividing k by exposure time the area erosion rate k' [%/s] is determined.

Fig. 12 shows the pit distribution indicated by k. Flow velocity effect is shown in Fig. 13 with the value k'.

1.5.3 *Volume Loss Rate*

Average depth of erosion pits d_m is obtained from the measurement of surface roughness of test specimens. From the micrographics of the erosion pits, we can determine the average radius r_m of the pits. Investigating these values it was found that d_m/r_m was in the order of $10^{-2} \sim 10^{-1}$.

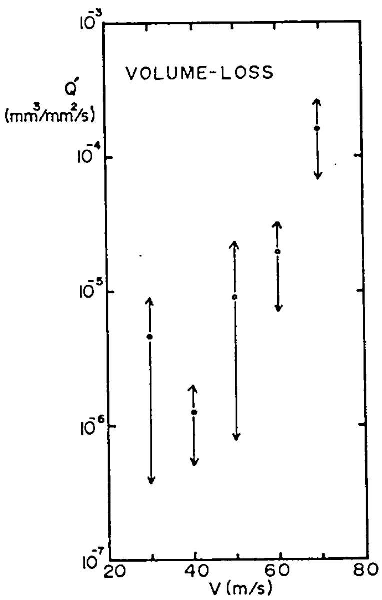

Fig. 14 Damage intensity Q'

$$d_m/r_m \sim 10^{-1\sim-2}$$

Under the assumption of conical pit, volume loss rate Q' [$mm^3/mm^2/s$] is calculated as follows.

$$Q' = \frac{k'}{\pi r_m^2} \times \frac{\pi d_m}{3} r_m^3 \times 10^{-2}$$
$$= \frac{1}{3} k' d_m \times 10^{-2} \qquad [mm^3/mm^2/s]$$

Relation between Q' and V are shown in Fig. 14.

2. Considerations on Experimental Results

2.1 *Space Distribution of Erosion Pits*

Figs. 10 and 12 show the typical distribution of the erosion pits indicated by N [$1/10^{-2}$ mm^2] and k [%] respectively. The erosion pits appear to concentrate near the end of the fixed-cavity marked ▲ in each figure. The same results was also obtained under other flow velocities. From this we can confirm that the collapse of bubbles takes place near the end of the fixed-cavity and erosion pits are generated there.

As to the wide spread of the distribution, following items are considered to be effective. Firstly, pits situated on the head of test specimens are supposed to be generated by collision with small metal particles in test water. It is very difficult to remove these small particles thoroughly.

Two facts are considered to contribute to the spread of the distribution near its peak. One is the dispersion of collapse location due to different radii of bubbles. Calculation of bubble radius described in next section shows that the difference of collapsing time between two bubbles with initial radius $R_0=0.1$ and 1.0 mm is 3.4×10^{-5} sec. under the condition $V=30$ m/s. Then larger bubble travels longer distance than that of smaller one by

$$3.4\times10^{-5}\times3\times10^{4} \fallingdotseq 1.0 \quad [mm].$$

This value can explain partly the spread of the pit distribution. But the lack of the data about the initial radius and location of bubbles makes it impossible to discuss more in detail.

The other is the oscillation of the fixed-cavity end. From the record of the length of the fixed-cavity shown in Fig. 15, we can see that the end moves fore and aft with amplitude of about 2 mm. With the assumption that erosion pits are generated at the end of the cavity, this oscillation explains also part of the pit distribution.

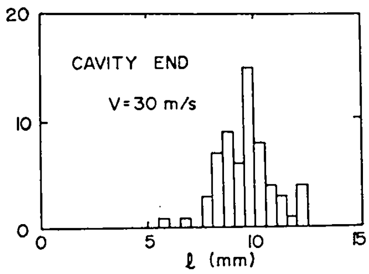

Fig. 15 Record of cavity length

We are now not yet in the position to conclude which of the above mentioned two reasonings is more prevailing. In order to discuss the position of cavitation erosion more precisely we must detect the physical properties of the end of fixed-cavity using a high speed camera, for example, and observe the behaviour of collapsing bubbles in detail.

2.2 *Flow Velocity Effects on Damage Intensity*

Damage intensity has a tendency to increase with flow velocity. Quantitative relation differs, however, according to the chosen parameter of the erosion as seen in the following.

In the first place, the following relation is obtained from Fig. 11:

$$N' \propto V^{5\sim6} \qquad (2.1)$$

This relation fits fairly well to the experimental results at CIT as well, which were obtained the flow velocity less than 30 m/s.

Flow velocity effect on damage intensity indicated by the area erosion rate k' [%/s] is shown in Fig. 13. The following relation is observed from this figure:

$$k' \propto e^{V} \qquad (2.2)$$

In Fig. 14 the flow velocity effect is indicated by volume loss rate Q' [$mm^3/mm^2/s$]. Though the accuracy of surface roughness makes plotted points scattered, the following relation will be considered to hold roughly:

$$Q' \propto e^V \tag{2.3}$$

Flow velocity is one of the most important hydrodynamic factors influencing upon cavitation erosion. In the next section we try a simplified theoretical investigation about the effect of flow velocity.

3. Simplified Solution of Bubble Radius Equation and Calculation of Pressure Field Around A Collapsing Bubble

3.1 *Bubble Radius Equation and its Solution*

Let the origin 0 be the center of a collapsing bubble which is assumed spherical in the whole collapsing process. The fluid motion is assumed to have spherical symmetry. Euler's equation of motion is described as follows, neglecting external forces:

$$\frac{\partial u}{\partial t}+u\frac{\partial u}{\partial r}+\frac{1}{\rho}\frac{\partial p}{\partial r}=0 \tag{3.1}$$

where u: flow velocity in outward radial direction
p: fluid pressure
ρ: density of water
r: distance from origin
t: time

Under the assumption of irrotational motion

$$u=\frac{\partial \phi}{\partial r} \tag{3.2}$$

$$\therefore \quad \frac{\partial}{\partial t}\left(\frac{\partial \phi}{\partial r}\right)+u\frac{\partial u}{\partial r}+\frac{1}{\rho}\frac{\partial p}{\partial r}=0 \tag{3.3}$$

where ϕ is velocity potential.
Integrating (3.3) with respect to r obtain the following expression.

$$\frac{\partial \phi}{\partial t}+\frac{1}{2}u^2+\int_{p_\infty}^{p}\frac{\partial p}{\partial r}=0 \tag{3.4}$$

Combining eqs. (3.3) and (3.4) the following expression is obtained.

$$ru\frac{\partial u}{\partial t}+\frac{r}{\rho}\frac{\partial p}{\partial t}+\frac{cu^2}{2}+c\int_{p_\infty}^{p}\frac{dp}{\rho}+cru\frac{\partial u}{\partial r}+\frac{cr}{\rho}\frac{\partial p}{\partial r}=0 \tag{3.5}$$

Pressure P and velocity U on the bubble wall must satisfis following relations.

$$\frac{dP}{dt}=\frac{\partial p}{\partial t}+U\frac{\partial p}{\partial r} \tag{3.6}$$

$$\frac{dU}{dt}=\frac{\partial u}{\partial t}+U\frac{\partial u}{\partial t} \tag{3.7}$$

In addition the law of conservation of mass is expressed as follows:

$$\frac{1}{\rho c^2}\frac{\partial p}{\partial t}+\frac{u}{\rho c^2}\frac{\partial p}{\partial r}+\frac{\partial u}{\partial r}+\frac{2u}{r}=0 \tag{3.8}$$

where c is the velocity of sound in water given by the next formula:

$$c^2=\frac{dp}{d\rho} \tag{3.9}$$

From eqs. (3.5), (3.6), (3.7) and (3.8), we obtain

$$RU\frac{dU}{dR}\left(1-\frac{2U}{c}\right)+\frac{3}{2}U^2\left(1-\frac{4U}{3c}\right)=\frac{R}{\rho U}\frac{dP}{dt}\left(\frac{U}{c}-\frac{U^2}{c^2}+\frac{U^3}{c^3}\right)+\int_{p_\infty}^{p}\frac{dp}{\rho} \tag{3.10}$$

Assuming that U is small enough compared with c and change of ρ is negligible, simplified bubble radius equation is obtained as follows:[4]

$$RU\frac{dU}{dR}\left(1-\frac{2U}{c}\right)+\frac{3}{2}U^2\left(1-\frac{4U}{3c}\right)=\frac{RU}{\rho c}\frac{dP}{dR}+\frac{P-p_\infty}{\rho} \tag{3.11}$$

In eq. (3.11) pressure of the bubble wall P is assumed to be given in the following form.

$$P=-\frac{\rho}{2}V^2C_p-\frac{2\sigma}{R}+P_0\left(\frac{R_0}{R}\right)^{3\gamma} \tag{3.12}$$

where V: velocity of main stream
C_p: non dimensional pressure around the bubble

$$C_p=p_b\Big/\left(\frac{1}{2}\rho V^2\right)$$

p_b: pressure around the bubble
p_0: initial value of internal pressure of the bubble

R_0: initial value of bubble radius
σ: surface tension of water
$\gamma=c_p/c_v$
c_p: specific heat of constant pressure
c_v: specific heat of constant volume

Gas in the collapsing bubble is assumed to change adiabatically. Substituting eq. (3.12) into eq. (3.11) we obtain the relation

$$RU\frac{dU}{dR}\left(1-\frac{2U}{c}\right)+\frac{3}{2}U^2\left(1-\frac{4U}{3c}\right)=\frac{RU}{\rho c}\frac{dP}{dR}+\frac{1}{\rho}\left[-\frac{\rho}{2}V^2C_p-\frac{2\sigma}{R}+P_0R_0^3\ R^{-3\gamma}\right]-\frac{p_\infty}{\rho} \tag{3.13}$$

Neglecting the first term of right side of eq. (3.13) and assuming $U/c\ll1$ except the final stage of collapsing, the following expression is obtained.

$$RU\frac{dU}{dR}+\frac{3}{2}U^2=-\frac{V^2}{2}C_p-\frac{2\sigma}{\rho}\frac{1}{R}+\frac{P_0R_0^{3\gamma}}{\rho}\frac{1}{R^{3\gamma}}-\frac{p_\infty}{\rho}=AR^{-3\gamma}+BR^{-1}+C \tag{3.14}$$

where $A=P_0R_0^{3\gamma}/\rho$
$B=-2\sigma/\rho$
$C=-V^2C_p/2-p_\infty/\rho$

Rearranging eq. (3.14) in the following form.

$$U\frac{dU}{dR}=\frac{F(R)}{2}U^2+\frac{G(R)}{2}$$
$$F(R)=-3/R \tag{3.15}$$
$$G(R)=2(AR^{-3\gamma-1}+BR^{-2}+CR^{-1})$$

and putting

$$z=U^2\quad(z\geqq0) \tag{3.16}$$

(3.14) is transformed into a first order linear differential equation,

$$\frac{dz}{dR}-F(R)\cdot z=G(R) \tag{3.17}$$

from which general solution is easily obtained as follows:

$$z(R)=2\left[\frac{A}{-3(\gamma-1)}R^{-3\gamma}+\frac{B}{2}R^{-1}+\frac{C}{3}\right]+\frac{N}{R^3} \tag{3.18}$$

where N is integration constant.

Using nondimensional variable β which is defined as

$$\beta=R/R_0\quad(0<\beta\leqq1) \tag{3.19}$$

solution (3.18) is rewritten as follows:

$$z(\beta)=2\left[\frac{A}{-3(\gamma-1)R_0^{3\gamma}}\beta^{-3\gamma}+\frac{B}{2R_0}\beta^{-1}+\frac{C}{3}\right]+\frac{N}{R_0^3}\beta^{-3} \tag{3.20}$$

If we assume the initial velocity of the bubble wall U to be zero, the final solution is as follows,

$$z(\beta)=2\left[\frac{A}{-3(\gamma-1)R_0^{3\gamma}}\beta^{-3\gamma}+\frac{B}{2R_0}\beta^{-1}+\frac{C}{3}\right]-2\beta^{-3}\left[\frac{A}{-3(\gamma-1)R_0^{3\gamma}}+\frac{B}{2R_0}+\frac{C}{3}\right] \tag{3.21}$$

Velocity of the bubble wall is given as follows:

$$U(\beta)=-\sqrt{z(\beta)} \tag{3.22}$$

leading to the expression for the acceleration of the bubble wall $\dot{U}(\beta)$.

$$\dot{U}(\beta)=\frac{dU}{dt}=\frac{dU}{d\beta}\cdot\frac{d\beta}{dt}=\frac{1}{R_0}\left[\left[\frac{\gamma A}{(\gamma-1)R_0^{3\gamma}}\beta^{-3\gamma-1}-\frac{B}{2R_0}\beta^{-2}\right]+3\beta^{-4}\left[\frac{A}{-3(\gamma-1)R_0^{3\gamma}}+\frac{B}{2R_0}+\frac{C}{3}\right]\right] \tag{3.23}$$

These equations (3.21), (3.22) and (3.23) describe the motion of the bubble wall.

3.2 *Calculation of Pressure Field Around A Collapsing Bubble*

Substituting equation of continuity[5)]

$$ur^2=UR^2 \tag{3.24}$$

into (3-1), we get the expression

$$\frac{1}{\rho}\frac{dp}{dr}=-\frac{1}{r^2}\left(2RU^2+R^2\frac{dU}{dt}\right)-u\frac{\partial u}{\partial t} \tag{3.25}$$

Integrating (3.25) with respect to r, under the condition $u|_{r=\infty}=0$, the following relation is obtained.

$$\frac{1}{\rho}(p-p_\infty)=\left(2RU^2+R^2\frac{dU}{dt}\right)\frac{1}{r}-\frac{u^2}{2}$$
$$=\frac{1}{r}[2Rz(\beta)+R^2\dot{U}(\beta)]-\frac{1}{2}\frac{R^4}{r^4}z(\beta)$$
$$\frac{p}{p_\infty}-1=\frac{\rho}{p_\infty}z(\beta)\left[\frac{2R_0\beta}{r}-\frac{R_0^4\beta^4}{2r^4}\right]+\frac{\rho R_0^2\beta^2}{p_\infty r}\dot{U}(\beta) \tag{3.26}$$

By using eq. (3.26) we can calculate pressure field around the collapsing bubble.

3.3 *Change of Bubble Radius*

Minimum value of bubble wall velocity $U_{\min}(U_{\min}<0)$ is obtained from the equation

$$\dot{U}(\beta)=0 \tag{3.27}$$

Using nondimensional bubble wall velocity $\bar{U}$ defined as

$$\bar{U}=U/U_{\min} \tag{3.28}$$

we get the relation between nondimensional time τ and bubble radius ratio β as follows:

$$\tau=\frac{-U_{\min}}{R_0}t \quad (0<\tau)$$
$$=\int_1^\beta \frac{d\beta}{-\bar{U}} \tag{3.29}$$

3.4. *Numerical Calculations*

In numerical calculation of expressions (3.21), (3.22) and (3.26), P_0 is given as vapour pressure at 20°C and pressure at infinity p_∞ is given as the pressure in the tunnel. Pressure coefficient C_p taken as -0.1, and initial radius $R_0=0.1$ mm. Calculation of eq. (3.23) is stopped when the sign of $\dot{U}(\beta)$ changes.

Fig. 16 is the calculated pressure field around the collapsing bubble under the condition $V=50$ m/s. The location of bubble wall is shown by broken line and attached numbers are nondimensional time $\tau\times10^2$.

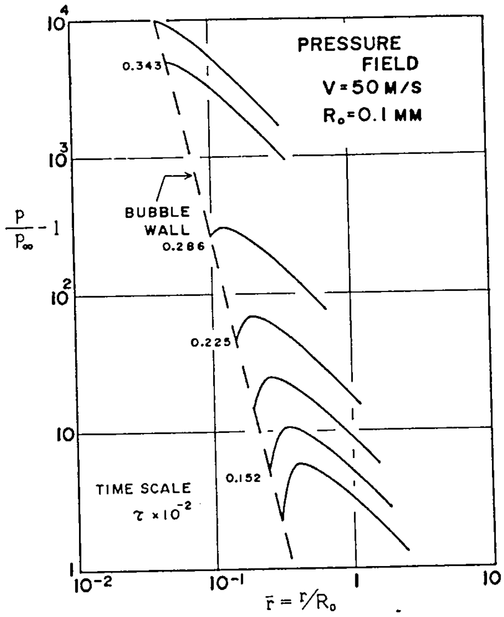

Fig. 16 Pressure field around a collapsing bubble (calculation)

From these calculations it is known that the pressure field has its peak at the point slightly outside of the bubble wall and this peak approaches to the bubble wall with the progress of collapse. At the final stage of collapse value of pressure peak attains $10^2\sim10^5$ times as high as the pressure at infinity p_∞, and it attenuates with distance from the bubble wall.

With this result we expect that the bubble collapse near the specimen surface can supply high enough energy to generate erosion pits.

Fig. 17 shows the relation between non-

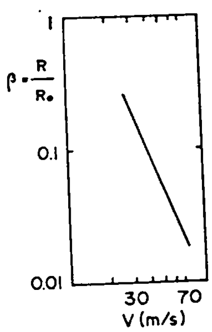

Fig. 17 Minimum radius of a bubble

dimensional bubble radius at the final stage of collapse and flow velocity. With increasing flow velocity, the minimum radius of a bubble decreases rapidly for the same initial radius. This is caused by a growth of the first term of right side of eq. (3.14) in proportion to V^2.

4. Consideration on the Flow Velocity Effect on Damage Intensity

As described in 2.2, different parameters of damage intensity derive different expressions for flow velocity effect. It is difficult to conclude which expression is most adequate, however, some consideration into this problem will be described in the following.

Velocity of the bubble wall U and pressure around the collapsing bubble are the values which have close connection with damage intensity. Assuming that damage intensity increases in proportion to impulse provided to surface of materials, the following expression is obtained.

$$(\text{damage intensity}) \propto \int_0^{\tau_1} p d\tau \qquad (4.1)$$

where τ_1: time interval from the start of bubble collapse to the time when $\dot{U}$ becomes zero

Fig. 18 shows the maximum values of U in term of Mach number M_m as a function of V. From this figure we obtain the relation:

$$M_m \propto V^5 \qquad (4.2)$$

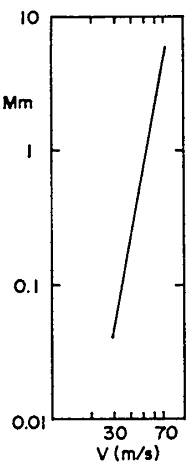

Fig. 18 Maximum velocity of the bubble wall

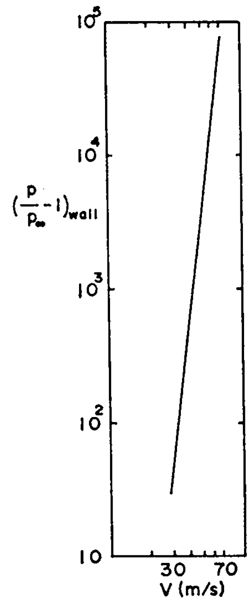

Fig. 19 Maximum pressure around a collapsing bubble

The maximum value of p is shown in Fig. 19 giving the following relation:

$$\left(\frac{p}{p_\infty}-1\right) \propto V^{11} \qquad (4.3)$$

Now the collapsing time τ is supposed to have the following relation:

$$\tau \propto 1/U \propto V^{-5} \qquad (4.4)$$

With the expressions (4.1), (4.3) and (4.4), therefore, we obtain the following result:

$$(\text{damage intensity}) \propto V^{11} \times V^{-5} = V^6 \qquad (4.5)$$

Under the assumption (4.1), the relation (4.5) shows good agreement with experimental result (2.1).

5. Conclusions

The results obtained in the previous sections are summarized as follows:

(1) Cavitation erosion is deeply affected by flow velocity. The number of erosion pits increases in proportion to the 5th to 6th power of flow velocity and eroded area in proportion to e^V.

(2) Cavitation erosion are generated near the end of fixed-cavity.

(3) The length of fixed-cavity varies over a range of 7 mm when its mean value is 10 mm, and this is one of the main factor of wide spread of erosion pits.
(4) The maximum value of the velocity of the bubble wall and pressure around the bubble derived from simplified equation of bubble radius increase in proportion to the 5th and the 11th power of flow velocity.

Under the assumption that damage intensity increases in proportion to the impulse provided to the surface of specimens, calculated results mentioned in (4) shows good agreement with the experimental relation between the number of erosion pits and flow velocity.

In carrying out this experimental study we were supported by many specialists in the field of hydrodynamics and material science. We should like to thank T. Komura, M. Maeda, S. Mineyama and the postgraduate students in our laboratory for their helpful suggestions and assistance in the experiments. The authors were favored to have the considerable assistance and kind guidance of Prof. Dr. K. Iida and H. Nagai in taking micrographics, which was highly appreciated.

We are also deeply indebted to T. Suzuki, S. Sasaya and H. Nishiogi for their assistance in preparting test specimens.

HITAC-8700/8800 at the Computer Center of University of Tokyo was used throughout for the numerical calculations.

References

1) Y. UKON, S. TAMIYA and H. KATO: On the Transient Cavitation, Journal of the Society of Naval Architects of Japan, Vol. 130, pp. 51-62, December, (1971), (in Japanese)
2) H. MIYATA, S. TAMIYA and H. KATO: Some Characteristics of a Partially Cavitating Hydrofoil, Journal of the Society of Naval Architects of Japan, Vol. 132, pp. 99-105, December, (1972), (in Japanese)
3) R. T. KNAPP: Recent Investigations of the Mechanics of Cavitation and Cavitation Damage, Trans. ASME, Vol. 77, pp. 1045-1054, (1970)
4) R.T. KNAPP et al.: *Cavitation*, p. 113, (McGraw-Hill Book Company, 1970)
5) L. RAYLEIGH: On the Pressure Developed in a Liquid During the Collapse of a Spherical Cavity, Phil. Mag. Vol. 34, pp. 94-98, (1871)
6) B.C. SYAMALA RAO, et. al.: Cavitation Studies with Venturi and Rotation Disk in Water, Trans. ASME, pp. 563-579, (1970)